Progress In Electromagnetics Research M, Vol. 107, 119–129, 2022

A Parasitic Array Based Pattern Reconfigurable Patch Antenna for Wi-Fi 6E Application

Bhaben Saikia and Kunal Borah*

Abstract—A pattern reconfigurable microstrip patch antenna with two parallel parasitic patches placed close to both sides of a rectangular driven patch is investigated and presented in this article. Four switchable shorting posts are used to enable the parasitic elements to act either as a reflector or director for beam reconfiguration, based on the operating state of four associated PIN diode switches. To avoid large change in the dimension of both parasitic patch and ground plane, and minimize its effect on beam steerability and return loss, two PIN diodes are placed on the top face and the other two on the slots etched on the ground plane. Radiation pattern of the proposed antenna can be reconfigured into four distinct directions in the H-plane with radiation maximum at $+40°$, $0°$, $-40°$, and $\pm 45°$. With overall compact dimension of $(35 \times 55)\,\text{mm}^2$ and acceptable return loss for all reconfigurable modes around 6.2 GHz frequency, the proposed antenna is a potential candidate for Wi-Fi 6E application. The measured peak gain varies between 3.9 dBi and 5.2 dBi with an average of 4.6 dBi for all beam tilt angles. Consistency between the simulated and experimental results validates the design theory and its promising application.

1. INTRODUCTION

Modern multifunctional high-speed wireless communications demand antenna with flexible radiation characteristics to adapt to the alteration of operating environment. Therefore, reconfigurable antennas have received significant attention in recent years as they offer diversities in terms of resonant frequency, bandwidth, radiation pattern, and polarization characteristics [1]. Pattern reconfigurable or beam steerable antenna is a prime candidate for research in the field of reconfigurable antenna, because reconfigurability in the radiation pattern contributes to noise avoidance, minimization of co-channel interference, and multipath propagation fading by directing signal only towards the desired coverage area and maneuvering away from unwanted directions which is very crucial for efficient utilization of allotted bands for different wireless services such as WiMAX and Wi-Fi [2]. Thus, the improvement in data security, spectral efficiency, and transmission data rate can be achieved to enhance the overall performance of the wireless system [3, 4]. Bulky size, requirement of expensive and complex phase shifting circuits and power divider unit limit the utility of classical phased antenna array technique to achieve the beam steerability for mobile wireless devices [5–8]. Modification in the antenna structures for beam reconfiguration by sole use of RF switches on different positions of the radiating element also results in the alteration of their resonant frequency along with other radiation characteristics [9–11]. Due to the limitations of these two techniques, many pattern reconfigurable antennas based on Yagi-Uda antenna radiation principle have been reported in recent years. These antennas employ parasitic elements as a director or reflector which surrounds the driven element [12–15].

Received 1 December 2021, Accepted 6 January 2022, Scheduled 12 January 2022
* Corresponding author: Kunal Borah (kbnerist@gmail.com).
The authors are with the Department of Physics, North Eastern Regional Institute of Science and Technology (Deemed to-be-University), Nirjuli, Itanagar, Arunachal Pradesh 791109, India.

In [14], two parasitic strips are placed on both sides of a driven strip, and each parasitic strip is loaded with RF switches. These switches alter the parasitic strip length upon activation to act as either a reflector and director and produce beam reconfiguration at $+35°$, $0°$, and $-35°$ in the H-plane. A beam steerable monopole antenna mounted on an octagonal copper board with eight concentric parasitic structures is demonstrated in [15], and RF switches are used to connect and disconnect these parasitic structures. These parasitic elements work as director and reflector on switching, and beam tilting is achieved. Four slot loaded parasitic patches placed on left and right sides of a driven patch are presented in [16] for pattern reconfiguration at $-7°$, $+33.5°$, and $-40°$ in the E-plane. Three switches are mounted on the slots of each parasitic patch to change their physical dimension to work as either reflector or director. However, a total of twelve switches are used in the design, and measurement is carried out using metallic strip as an ideal switch instead of practical RF switch. An antenna with reconfigurable radiation maximum consists of a central driven patch, and two vertically placed parasitic patches are proposed in [17] for Ka-band satellite applications. Switching of MEMS switches between the driven and parasitic patches results in reconfigurable major lobe orientation in the H-plane at $+17°$, $-25.8°$, $+3.5°$, and $+0.7°$. In [18], a pattern reconfigurable antenna capable of changing its radiation pattern from omnidirectional to directional mode, with the help of two arc-shaped parasitic stubs placed on the back side of the antenna is demonstrated for WLAN and WiMAX applications. The reconfigurable antenna reported in [19] uses single feed line to excite two rotatable patches through PIN diode switches. Mechanical rotation of the excited patches produces beam reconfiguration between $+30°$ and $-30°$ directions. In [20], a beam steerable patch antenna is proposed for beam steering at $+30°$, $0°$, and $-30°$. A 5×5 parasitic pixel layer is placed above the driven patch, and 20 ideal switches are used to make electrical connection between them to alter the pixel geometry and achieve pattern reconfiguration. A beam steerable parasitic array antenna based on two embedded PIN diodes is reported in [21] for beam steering angles of $+30°$, $0°$, and $-30°$. Many parasitic element-based pattern reconfigurable patch antennas (PRPAs) discussed earlier have used a large number of ideal switches, and the investigation of beam steering is not reported with the implementation of practical RF switch in the fabrication [16, 18, 20]. The research gap related to beam steering patch antenna for Wi-Fi 6E band (5.925 GHz–6.425 GHz) application as found in extensive literature survey is addressed in this article.

This article presents a PIN diode-based pattern reconfigurable parasitic array antenna with an inimitable shorting post geometry and simple DC biasing circuitry. Two PIN diodes are placed at the top side, and two PIN diodes are mounted on the slots etched on the ground plane, to activate and deactivate the shorting posts. This technique is employed to avoid large change in the dimensions of both parasitic patch and ground plane, and minimize its effect on beam steerability and return loss. For all four beam steerable modes, measured resonant frequencies of the fabricated antenna are found around 6.2 GHz, which almost covers the Wi-Fi 6E band (5.925–6.425 GHz).

2. ANTENNA DESIGN AND RECONFIGURATION MECHANISM

The proposed PRPA synthesized on an FR4 substrate ($\varepsilon_r = 4.4$) of dimension $(35 \times 55 \times 1.6)\,\text{mm}^3$ is illustrated in Figure 1. As shown in Figure 1, the proposed antenna has two parallel rectangular parasitic patch elements adjacent to each non-radiating edge of a driven patch. The dimension of driven patch is calculated using the transmission line model (TLM) of patch antenna [23] and found as $L = 11.59\,\text{mm}$ and $W = 15.49\,\text{mm}$ for 6 GHz resonant frequency. The driven patch is excited with an optimized inset feed microstrip line of dimension $(16.6 \times 0.8)\,\text{mm}^2$ for the best impedance matching over the desired Wi-Fi 6E band (5.925 GHz–6.425 GHz). The optimized dimension of parasitic patch element is smaller than the driven patch which has length $L_1 = 11.47\,\text{mm}$ and width $W_1 = 15.43\,\text{mm}$. Four shorting posts namely post 1, post 2, post 3, and post 4 of radius 0.7 mm are inserted in the parasitic elements to establish electrical connection with the ground plane via RF PIN diodes PD1, PD2, PD3, and PD4, respectively. Unlike the conventional method, post 1 and post 2 are positioned outside the parasitic elements, at a distance = 3.5 mm from radiating edge, and PD1 and PD2 are inserted in the gap as shown in Figure 1(a). For the activation of PD1 and PD2, DC bias wires are connected from bottom of the antenna via hole to minimize possible disturbances in the far field radiation characteristics. Three 10 pF SMD capacitors are mounted on three small rectangular slots etched on each parasitic element for DC blocking. Shorting post 3 is located at $u_1 = 6.2\,\text{mm}$, $v_1 = 1.7\,\text{mm}$ of parasitic element 1 while post 4

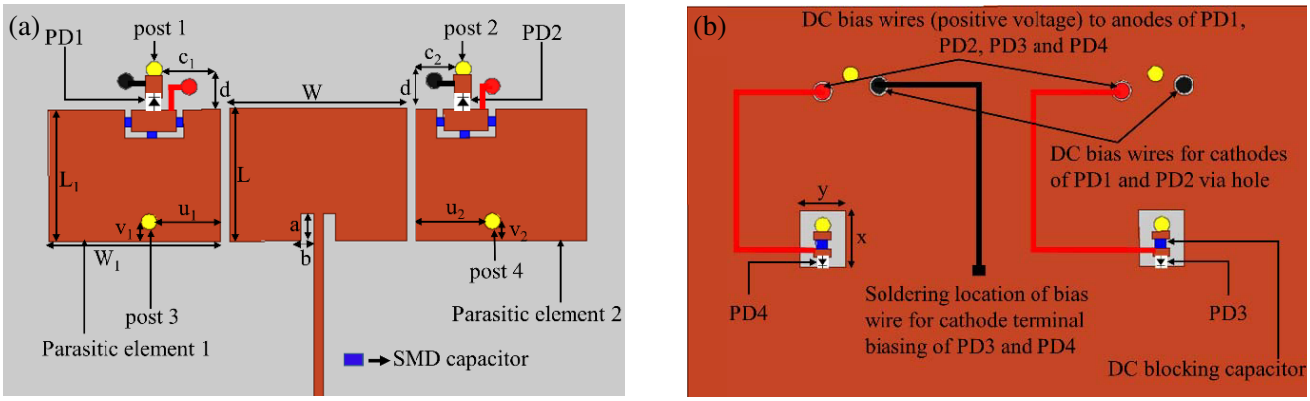

Figure 1. (a) Front side, (b) back side of the proposed antenna geometry.

is inserted on parasitic element 2 at position $u_2 = 6.7\,\text{mm}$, $v_2 = 1.7\,\text{mm}$. PIN diodes PD3 and PD4 are placed at the slot graved on the ground plane to establish electrical connection between the post and ground plane copper layer, which make the shorting post functional as depicted in Figure 1(b). The DC voltage applied to PD3 and PD4 for switching is blocked by two 10 pF SMD capacitors, preventing any interference with RF from the parasitic elements. As the location of shorting post plays a significant role in the beam steering process of PRPAs based on parasitic array, positions of all four shorting posts are optimized to maximize beam tilt angles. Optimal values of the design parameters are given in Table 1.

Table 1. Optimal values of design parameter.

Driven patch	$L = 11.59\,\text{mm}$	$W = 15.49\,\text{mm}$
Parasitic element	$L_1 = 11.47\,\text{mm}$	$W_1 = 15.43\,\text{mm}$
Inset dimension	$a = 2.4\,\text{mm}$	$b = 1.1\,\text{mm}$
Position of shorting post 1	$c_1 = 5.7\,\text{mm}$	$d = 3.5\,\text{mm}$
Position of shorting post 2	$c_2 = 4.2\,\text{mm}$	$d = 3.5\,\text{mm}$
Position of shorting post 3	$u_1 = 6.2\,\text{mm}$	$v_1 = 1.7\,\text{mm}$
Position of shorting post 4	$u_2 = 6.7\,\text{mm}$	$v_2 = 1.7\,\text{mm}$
Rectangular slot on ground	$x = 5\,\text{mm}$	$y = 4\,\text{mm}$

2.1. Reconfiguration Principle

When a parasitic element is placed adjacent to an excited patch, electromagnetic coupling induces a current in the element, and the distribution of this induced current determines the radiation characteristics such as gain and main lobe orientation of the array. In the proposed antenna, four shorting posts are inserted at optimum positions of the parasitic elements, and ON-OFF switching of RF PIN diode associated with each shorting post alters the induced current distribution along with effective electrical length of these elements. This causes the elements to perform their function either as reflector or director for beam steering which is identical to the radiation mechanism of Yagi-Uda antenna [12, 14]. For ON state operation of a PIN diode, the induced current flows from the parasitic element to the ground plane through the shorting post which, in turn, increases the electrical length of the element, and resonant length of the parasitic element becomes greater than driven patch length. This makes the parasitic element inductive and produces a phase shift in the induced current to reflect the radiated power away from the element, for its operation as a reflector. In contrast, the OFF state operation of PIN diode makes the resonant length of parasitic element smaller than the patch length,

since no induced current flows through the shorting post to reach the ground plane. The parasitic element now becomes capacitive and achieves desired phase shift in induced current to direct radiated power of the antenna towards the parasitic element (director).

In mode 1, PIN diodes PD2 and PD4 are turned ON while PD1 and PD3 remain in OFF state. Parasitic element on left of the driven patch acts as director while the right parasitic performs the function of reflector and deflects the H-plane radiated beam towards left. In mode 2, PD1 and PD3 are switched to operate in ON state while PD2 and PD4 are turned OFF. This reverses the functions of parasitic elements, and left parasitic element works as a reflector while right parasitic acts as a director. Thus, the H-plane main lobe is deflected towards right. In mode 3, both PD1 and PD2 are turned OFF which results in a bidirectional radiation pattern in the H-plane. All the PIN diodes PD1, PD2, PD3, and PD4 are turned ON for mode 4 operation, and the array radiates the beam in broadside direction.

2.2. Antenna Geometry Evolution

Stage 1:

In this stage, the proposed parasitic array structure is loaded with two shorting posts namely post 1 and post 2, one for each element. Unlike the conventional way of inserting shorting posts within parasitic elements, the shorting posts are positioned outside the elements as shown in Figure 2. These posts can

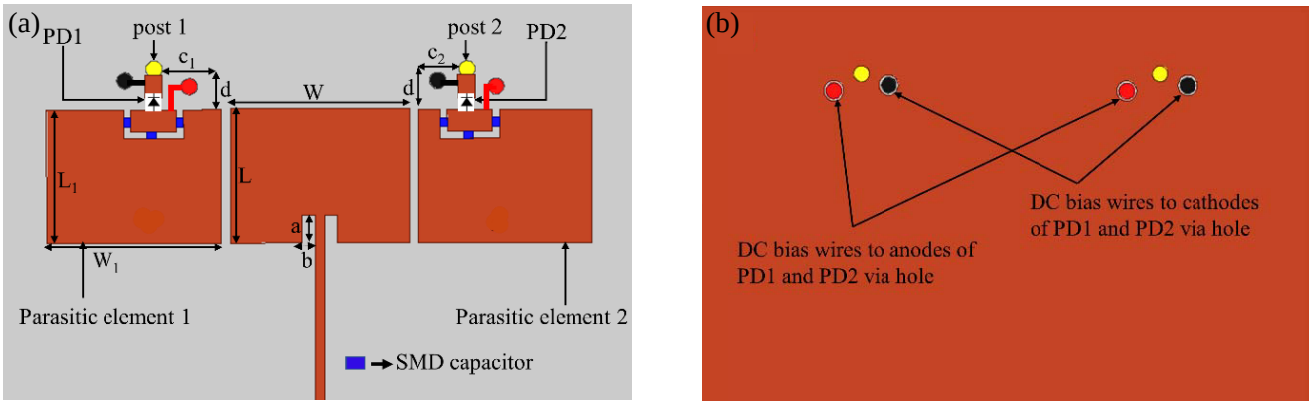

Figure 2. (a) Top, (b) bottom side of the antenna geometry at stage 1.

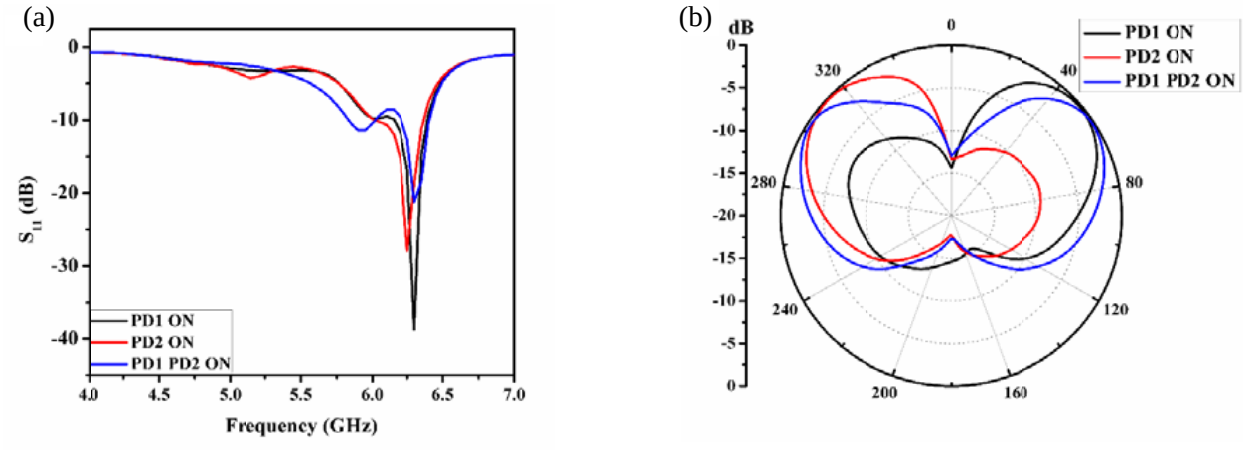

Figure 3. (a) Reflection coefficient, (b) H-plane pattern of the antenna in stage 1 (simulated).

be activated with ON state operation of PIN diodes PD1 and PD2 mounted in the gap between the parasitic elements and shorting posts. A total of six 10 pF SMD capacitors (Murata Electronics) are placed on the rectangular slots etched near PIN diode mounting positions of both parasitic elements for DC blocking purpose. DC bias wires are applied across PIN diode switches from bottom of the antenna via hole to avoid any possible disturbance in far field radiation characteristics of the antenna. The positions of shorting posts, parasitic element dimension, and spacing between the active and parasitic elements are adjusted for optimum beam tilt angle and reflection coefficient. From the simulation in High Frequency Structure Simulator (HFSS) ver. 13.0, three distinct beam reconfiguration modes are found with beam tilt angle at 50°, −50°, and ±60° in H-plane around 6.3 GHz frequency. Simulation results of reflection coefficient and H-plane radiation pattern for all three operating modes are illustrated in Figure 3. It is observed that the parasitic array steers the beam sufficiently which is evident from the obtained tilt angles, but beam steering is not achieved in the broadside direction. Moreover, side lobe is significantly large for the tilt angles at 50° and −50°.

Stage 2:

Since the antenna designed in the first stage is unable to steer the beam along the broadside direction in H-plane even after many series of optimization process, two additional shorting posts namely post 3 and post 4 are introduced in the parasitic elements to resolve this issue as shown in Figure 1. Unlike the shorting post arrangement of post 1 and post 2, post 3 and post 4 are inserted on the parasitic elements at locations (u_1, v_1) and (u_2, v_2), respectively. The posts are made switchable between open and short by mounting PIN diodes PD3 and PD4 on the rectangular slots etched on ground plane which control the electrical connection. The ON state operation of these PIN diodes establishes the electrical connection between the ground plane and shorting posts to make them functional. Two 10 pF SMD capacitors are inserted between the soldering pads on ground plane for DC isolation as shown in Figure 1(b). Thus, the final geometry of the proposed PRPA consists of four shorting posts, equal number of PIN diodes, and eight DC blocking SMD capacitors. This PRPA design is able to reconfigure the beam maximum at −45°, +45°, ±50°, and 0° in the H-plane. To the best of the authors' knowledge, no existing work based on a parasitic array structure similar to the proposed antenna [17, 21, 22] has reported beam reconfiguration at four distinct directions which covers from 45° to −45° in the H-plane, as achieved in this report.

The RF PIN diode employed in this design is SMP 1345-040LF, which is primarily chosen because of the attractive features such as tiny size, low forward resistance of only 1.5-Ω, and small reverse capacitance of 0.15 pF. For simulation, PIN diode is modeled as an RLC equivalent circuit with the information obtained from the manufacturer datasheet. In ON state, it is equivalent to series combination of an inductance $L_s = 0.45$ nH and resistance $R_s = 1.5\,\Omega$ while in OFF state, it is modeled with an inductance $L_s = 0.45$ nH which is in series with a parallel grouping of reverse resistance $R_p = 5\,\text{k}\Omega$ and capacitance $C_p = 0.15$ pF.

2.3. Parametric Study

Spacing between the driven and parasitic elements and size of parasitic element should be optimized for enhanced beam tilt angle and reflection coefficient S_{11}, which is carried out with HFSS by tuning one parameter at a time while keeping the other parameter constant. This optimization is done for mode 1 operation and is kept same for other modes.

2.3.1. Effect of Driven and Parasitic Element Spacing

Electromagnetic coupling is considered as an important factor for beam steering in the proposed PRPA, which depends on the spacing s between the active and parasitic elements. The radiation pattern and S_{11} graph shown in Figure 4 illustrates the effect of s for its different values. As s is changed in decremental order from 2 mm to 0.8 mm by step size of 0.4 mm, tilt angle increases from −30° to −45°, but the S_{11} value also increases drastically from −40 dB to −21 dB along with a decrease in gain by 0.3 dB. As tilt angle is the most desirable characteristic in this design, $s = 0.8$ mm is considered as the optimal value.

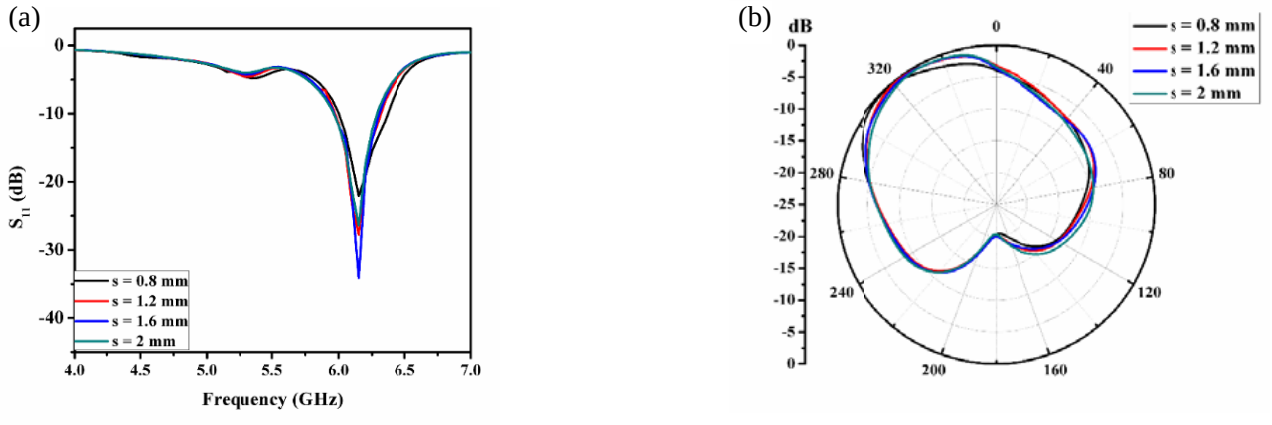

Figure 4. (a) S_{11} plot and (b) H-plane pattern, for various values of s.

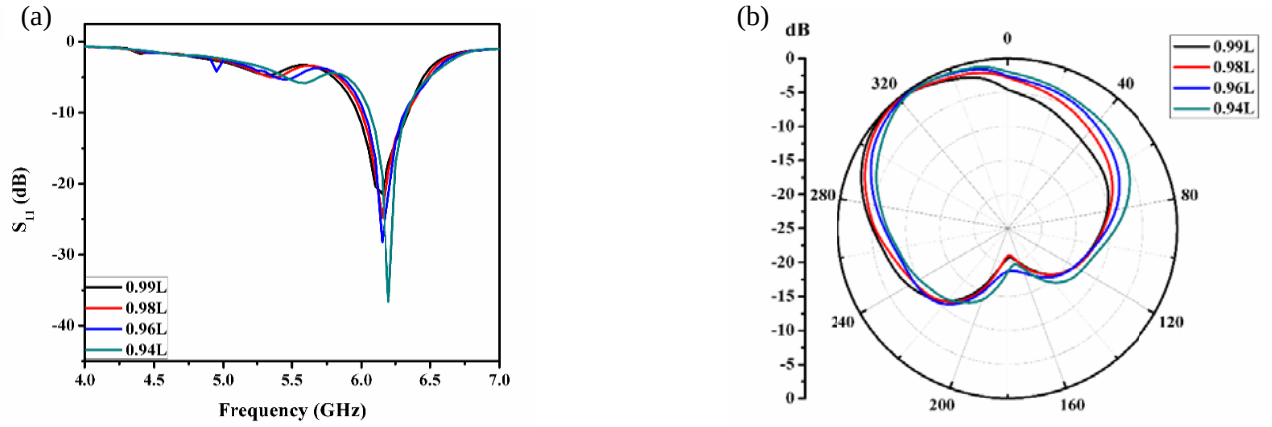

Figure 5. (a) S_{11} graph and (b) H-plane radiation pattern, for different values of L_1.

2.3.2. Effect of Parasitic Length

The effect of parasitic length L_1 on beam steering is also investigated for optimal values of beam tilt angle by changing L_1 as $0.99 \times L$, $0.98 \times L$, $0.96 \times L$, and $0.94 \times L$. From the simulation results, it is observed that as L_1 is decreased from $0.99 \times L$ to $0.94 \times L$, return loss S_{11} improves from -21 dB to -37 dB while tilt angle decreases from $-45°$ to $35°$. The front to back ratio is also found to follow a degrading trend with decrease in the parasitic length as shown in Figure 5. Hence, the optimal length of parasitic element is considered as $L_1 = 0.99 \times L$.

3. RESULT AND DISCUSSION

Figure 6 shows front and rear side photographs of the fabricated antenna. The return loss S_{11} and radiation pattern of the fabricated antenna are measured using Agilent N5247A vector network analyzer (VNA) and anechoic chamber measurement setup, respectively. VNA is calibrated using Thru-Reflect-Line (TRL) technique with a 3.5 SMA calibration kit. The distance between transmitter and receiver inside the anechoic chamber is 1.5-m while the transmitted power is in 13 to 15 dBm range. An Amkom horn antenna of 50-Ω impedance and (1–18) GHz frequency range is used as the reference antenna in gain measurement.

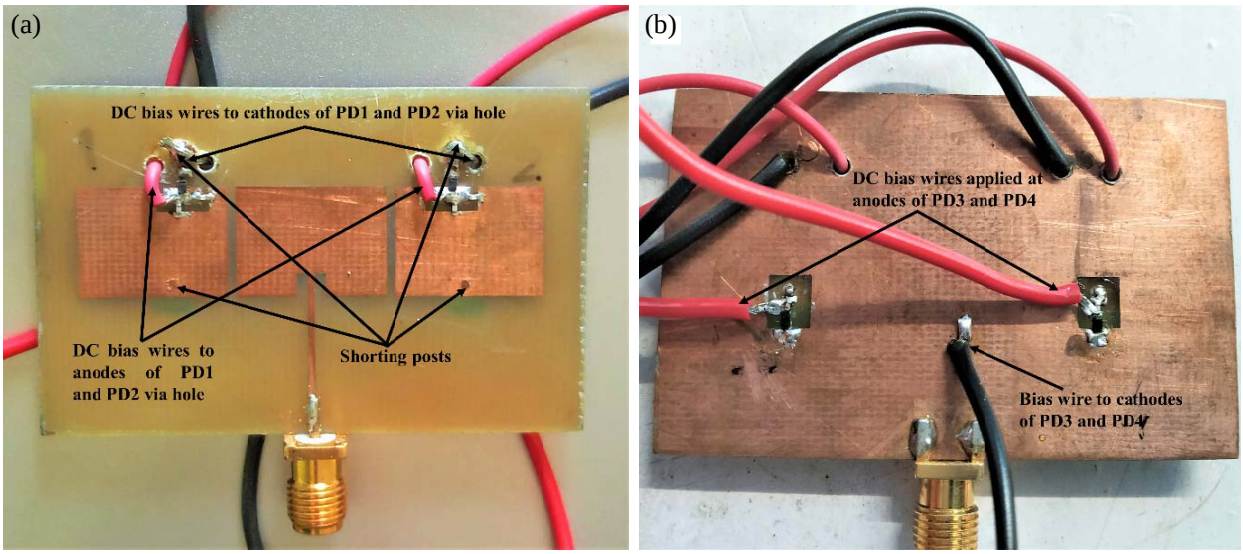

Figure 6. (a) Front, (b) rear view of the proposed fabricated antenna.

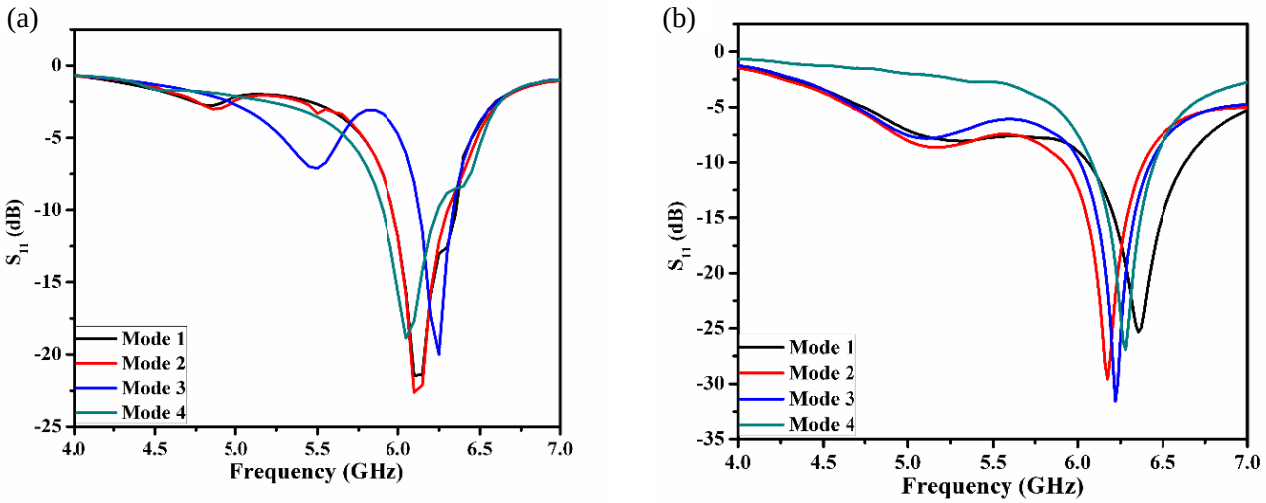

Figure 7. (a) Simulated, and (b) measured S_{11} plot for different modes of the proposed PRPA.

3.1. Return Loss S_{11} Measurement

The proposed PRPA is designed to operate in four different modes for steering the H plane radiation beam into four distinct directions. Resonant frequencies for mode 1, mode 2, mode 3, and mode 4 operations are measured at 6.35 GHz, 6.17 GHz, 6.22 GHz, and 6.28 GHz while their simulated counterparts are observed at 6.1 GHz, 6.1 GHz, 6.25 GHz, and 6.05 GHz, respectively, as shown in Figure 7. It is observed from the measured S_{11} that all reconfiguration modes almost cover the 5.925 GHz–6.425 GHz frequency bandwidth, dedicated for Wi-Fi 6E application. Simulation and measurement results of resonant frequency, S_{11}, and percentage bandwidth for various operating modes are compared in Table 2. Small variation can be observed between the simulated and measured values of S_{11} and -10 dB percentage bandwidth, which could be attributed to the fabrication tolerances and presence of actual components viz. PIN diodes, capacitors, and DC bias wires.

Table 2. Comparison of simulated and measured resonant frequency, S_{11} and -10 dB percentage bandwidth.

Modes of operation	Resonant frequency (GHz)		Reflection coefficient S_{11} (dB)		-10 dB percentage bandwidth	
	Simulated	Measured	Simulated	Measured	Simulated	Measured
Mode 1	6.1	6.35	-21.5	-25.3	6.89%	9.13%
Mode 2	6.1	6.17	-21.7	-29.6	6.23%	7.78%
Mode 3	6.25	6.22	-20	-31.6	3.52%	6.59%
Mode 4	6.05	6.28	-18.9	-26.9	5.79%	5.89%

3.2. Radiation Pattern and Gain Measurement

The measurement of H-plane radiation pattern of the fabricated antenna is performed in an anechoic chamber measurement setup for various operating modes and are depicted in Figure 8. From the comparative plot of normalized radiation pattern illustrated in Figure 8, it can be observed that measured radiation pattern of the fabricated antenna is almost identical to the simulated pattern and offers beam maximum diversities at $-40°$, $+40°$, $\pm 45°$, and $0°$. It is seen that measured tilt angle has dropped by $5°$ from the corresponding simulated values, which can be due to the presence of DC bias circuitry in the fabricated antenna.

The gain of the fabricated antenna is measured using conventional two antenna method, and the

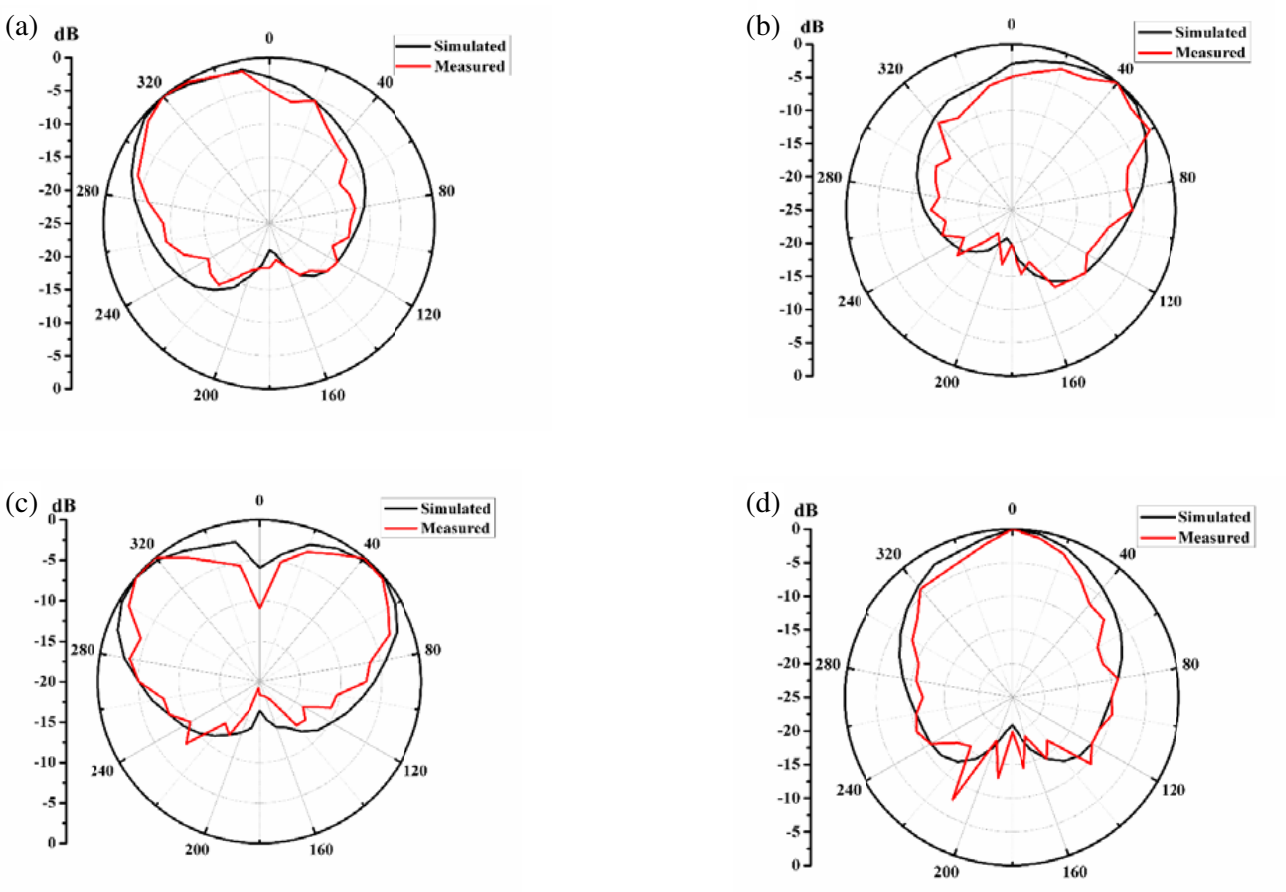

Figure 8. H-plane radiation pattern, (a) mode 1, (b) mode 2, (c) mode 3 and (d) mode 4.

Table 3. Simulated and measured results of beam tilt angle and antenna gain, and simulated antenna efficiency for various reconfiguration modes.

Mode of operation	Tilt angle		Antenna Gain (dBi)		Simulated efficiency (%)
	Simulated	Measured	Simulated	Measured	
Mode 1	-45°	-40°	5.2	4.7	79
Mode 2	$+45^\circ$	$+40^\circ$	5	4.6	78
Mode 3	$\pm 50^\circ$	$\pm 45^\circ$	4.3	3.9	71
Mode 4	0°	0°	5.5	5.2	82

Table 4. Comparison of the proposed PRPA with other relevant works (λ_0 is the free space wavelength at lowest resonant frequency).

Ref. No.	Overall Size (λ_0^2)	Switch type and Quantity		DC bias circuitry	Peak gain (dBi)	Beam tilt angles
[16]	0.93×1.86	Conductive strip	12	Not applicable	Not reported	-7°, $+33.5^\circ$, -40°
[17]	Not reported	MEMS	2	Not applicable	7.24	$+17^\circ$, -25.8°, $+3.5^\circ$, $+0.7^\circ$
[18]	0.32×0.32	Conductive strip	4	Not applicable	3.2	Omnidirectional, $+90^\circ$, -90°
[19]	0.47×0.81	PIN diode	2	Present	5.5	From $+30^\circ$ to -30°
[20]	1.12×1.12	Conductive strip	20	Not applicable	8	0°, $+30^\circ$, -30°
[21]	0.62×1.47	PIN diode	2	Present	6.5	0°, $+30^\circ$, -30°
This work	0.72×1.13	PIN diode	4	Present	4.7	0°, $+40^\circ$, -40°, $\pm 45^\circ$

average peak gain of 4.6 dBi is obtained. It is observed that the average value of measured gain varies by 0.4 dBi compared to the simulated values. The actual SMD components (PIN diodes and capacitors) and presence of solder bumps in the fabricated antenna can lead to such variations in gain [21, 24]. A comparison of simulation and measurement results of beam tilt angle and antenna gain, and simulated antenna efficiency are listed in Table 3.

Design and performance comparison of the proposed antenna with those in state-of-the-art literature is presented in Table 4.

4. CONCLUSION

A parasitic array antenna with switchable shorting posts for beam steering in the H-plane is reported in this article for Wi-Fi 6E portable devices. The fabricated antenna almost covers 5.925 GHz–6.425 GHz frequency bandwidth. The PIN diodes associated with the shorting posts control the current flow in the parasitic array, and hence effective electric length of the parasitic elements can be altered to perform their functions either as reflector or director. The unconventional approach in positioning the shorting posts yields beam coverage from -45° to $+45^\circ$ in this design. The investigated antenna shows stable resonant frequency around 6.2-GHz for all beam steering angles. Parametric studies carried out in antenna geometry evolution process clearly indicate that the gap between driven and parasitic element, and parasitic size have significant effect on beam tilt angle and gain of beam steerable parasitic array. The implementation of E-plane pattern reconfiguration in this design is the scope for future investigation.

REFERENCES

1. Chen, S. H., J. S. Row, and K. L. Wong, "Reconfigurable square-ring patch antenna with pattern diversity," *IEEE Transactions on Antennas and Propagation*, Vol. 55, 472–475, 2007.
2. Kang, W. S., J. A. Park, and Y. J. Yoon, "Simple reconfigurable antenna with radiation pattern," *Electronics Letters*, Vol. 44, 182–183, 2008.
3. Besoli, A. G. and F. D. Flaviis, "A multifunctional reconfigurable pixeled antenna using MEMS technology on printed circuit board," *IEEE Transactions on Antennas and Propagation*, Vol. 59, 4413–4424, 2011.
4. Ben Trad, I., J. M. Floc'h, H. Rmili, and F. Choubani, "A planar reconfigurable radiation pattern dipole antenna with reflectors and directors for wireless communication applications," *International Journal of Antennas and Propagation*, Vol. 2014, 1–10, 2014.
5. Sanyal, S., Q. Alfred, and T. Chakravarty, "A novel beam-switching algorithm for programmable phased array antenna," *Progress In Electromagnetics Research*, Vol. 60, 187–196, 2006.
6. Exposito-Dominguez, G., J.-M. F. Gonzalez, P. P. de La Torre, and M. Sierra-Castaner, "Dual circular polarized steering antenna for satellite communications in X band," *Progress In Electromagnetics Research*, Vol. 122, 61–76, 2012.
7. Yuan, T., N. Yuan, J. L.-W. Li, and M.-S. Leong, "Design and analysis of phased antenna array with low sidelobe by fast algorithm," *Progress In Electromagnetics Research*, Vol. 87, 131–147, 2008.
8. Mubasher, F., S. H. Wang, X. D. Chen, and Z. Ying, "Study of reconfigurable antennas for MIMO systems," *Proceedings of the 2010 International Workshop on Antenna Technology (iWAT'10)*, 1–4, IEEE, 2010.
9. Won Jung, C., M. J. Lee, G. P. Li, and F. D. Flaviis, "Reconfigurable scan-beam single-arm spiral antenna integrated with RF-MEMS switches," *IEEE Transactions on Antennas and Propagation*, Vol. 54, 455–463, 2006.
10. Sarrazin, J., Y. Mahé, S. Avrillon, and S. Toutain, "Pattern reconfigurable cubic antenna," *IEEE Transactions on Antennas and Propagation*, Vol. 57, 310–317, 2009.
11. Nikolaou, S., R. Bairavasubramanian, C. Lugo, I. Carrasquillo, D. C. Thompson, G. E. Ponchak, J. Papapolymerou, and M. M. Tentzeris, "Pattern and frequency reconfigurable annular slot antenna using PIN diodes," *IEEE Transactions on Antennas and Propagation*, Vol. 54, 439–448, 2006.
12. Huang, J. and A. C. Densmore, "Microstrip Yagi array antenna for mobile satellite vehicle application," *IEEE Transactions on Antennas and Propagation*, Vol. 39, 1024–1030, 1991.
13. Yang, X., B. Wang, S. Yeung, Q. Xue, and K. Man, "Circularly polarized reconfigurable crossed-Yagi patch antenna," *IEEE Antennas and Propagation Magazine*, Vol. 53, 65–80, 2011.
14. Zhang, S., G. Huff, J. Feng, and J. Bernhard, "A pattern reconfigurable microstrip parasitic array," *IEEE Transactions on Antennas and Propagation*, Vol. 52, 2773–2776, 2004.
15. Shi, Z., R. Zheng, J. Ding, and C. Guo, "A novel pattern-reconfigurable antenna using switched printed elements," *IEEE Antennas and Wireless Propagation Letters*, Vol. 11, 1100–1103, 2012.
16. Yang, X. S., B. Z. Wang, W. Wu, and S. Xiao, "Yagi patch antenna with dual-band and pattern reconfigurable characteristics," *IEEE Antennas and Wireless Propagation Letters*, Vol. 6, 168–171, 2007.
17. Deng, Z., J. Gan, H. Wei, H. Gong, and X. Guo, "Ka-band radiation pattern reconfigurable antenna based on microstrip MEMS switches," *Progress In Electromagnetics Research Letters*, Vol. 59, 93–99, 2016.
18. Koley, S., L. Murmu, and B. Pal, "A pattern reconfigurable antenna for WLAN and WiMAX systems," *Progress In Electromagnetics Research C*, Vol. 66, 183–190, 2016.
19. Khan, M. S., A. Iftikhar, A. D. Capobianco, R. M. Shubair, and B. Ijaz, "Pattern and frequency reconfiguration of patch antenna using PIN diodes," *Microwave and Optical Technology Letters*, Vol. 59, 2180–2185, 2017.

20. Li, Z., H. Mopidevi, O. Kaynar, and B. A. Cetiner, "Beam-steering antenna based on parasitic layer," *Electronics Letters*, Vol. 48, 59–60, 2012.
21. Sabapathy, T., M. F. B. Jamlos, R. B. Ahmad, M. Jusoh, M. I. Jais, and M. R. Kamarudin, "Electronically reconfigurable beam steering antenna using embedded RF PIN based parasitic arrays (ERPPA)," *Progress In Electromagnetics Research*, Vol. 140, 241–261, 2013.
22. Preston, S. L., D. V. Thiel, J. W. Lu, S. G. O'Keefe, and T. S. Bird, "Electronic beam steering using switched parasitic patch elements," *Electronics Letters*, Vol. 33, 7–8, 1997.
23. Balanis, C. A., *Antenna Theory: Analysis and Design*, John Wiley & Sons, 2015.
24. Allayioti, M., J. R. Kelly, and R. Mittra, "Beam and polarization reconfigurable microstrip antenna based on parasitics," *Microwave and Optical Technology Letters*, Vol. 60, No. 6, 1460–1464, 2018.